Journal of Materials Chemistry B

ROYAL SOCIETY OF CHEMISTRY

PAPER

View Article Online
View Journal | View Issue



Cite this: J. Mater. Chem. B, 2021, 9, 9900

# A unique self-reporting photosensitizer enabling simultaneous photodynamic therapy and real-time monitoring of phototheranostic process in a dynamic dual-color mode†

Dong-Hui Wang, [ab] Li-Jian Chen, [b] Xu Zhao [b] and Xiu-Ping Yan *[abc]

Phototheranostics has attracted great interest in cancer therapy. Small-molecule self-reporting photosensitizers, one kind of idea agent in phototheranostics, enables simultaneous photodynamic therapy (PDT) and feedback of therapeutic efficacy. However, previous such photosensitizers exclusively employed the change of single emission to monitor cell death, which can be disturbed by variations in photosensitizer concentration and the excitation intensity. Herein, we report a unique self-reporting photosensitizer **TPA-3PyA+** constructed from a twisted triphenylamine unit (TPA), three benzene ring units and three cyanovinyl-pyridinium units (PyA) for PDT and its real-time monitoring in a dynamic dual-color mode. **TPA-3PyA+** possesses a rotatable electron donor-π bridge-electron acceptor framework and exhibits high singlet oxygen quantum yield (124%) and a twisted intramolecular charge transfer (TICT) effect. **TPA-3PyA+** not only enables effective staining of cancer cells with dual-color fluorescence due to the TICT effect but also shows excellent PDT performance. The simultaneous change in emission color, intensity and intracellular location of **TPA-3PyA+** during cell death allows it to self-report cell death. Moreover, the change of dual-emission color allows distinguishing living and dead cells and effectively avoids interference in previous single-emission self-reporting photosensitizers. This work highlights the great potential of a self-reporting photosensitizer with dual-color emissions for efficient feedback of theranostics.

Received 24th September 2021,
Accepted 9th November 2021

DOI: 10.1039/d1tb02097h

rsc.li/materials-b



## Introduction

Cancer is the second most serious disease threatening human life, accounting for an estimated 10 million cancer deaths in 2020.[1] Nowadays, the development of precision theranostic techniques is one of the most attractive research areas in cancer treatment.[2–6] Phototheranostics is an advanced noninvasive theranostic technique as it shows good early diagnosis and therapy concurrently upon light-initiation.[7–10] Imaging-guided photodynamic therapy (PDT) attracts great interest due to its noninvasiveness, traceability and hypotoxicity.[11,12] However, conventional imaging-guided PDT cannot provide real-time feedback therapeutic responses, leading to the delay of treatment and over-treatment problems.[13–17] Advanced imaging-guided PDT, which employs a self-reporting photosensitizer system with a strong ability to produce toxic reactive oxygen species (ROS) and good fluorescence concurrently, can not only destroy cancer cells but also monitor the PDT process *in situ* in real-time.[18–21] In this way, excessive phototoxicity and other side effects induced by high irradiation intensity and drug overdose can be significantly reduced.

Small-molecule compounds are ideal candidates to construct self-reporting photosensitizers due to their clear composition and good stability. Self-reporting photosensitizers can be prepared by conjugating a photosensitizer and a fluorescent dye *via* a singlet oxygen ($^1O_2$) sensitive linker to kill cancer cells and real-time monitoring of the PDT process.[22,23] However, such conjugated photosensitizers are not easily developed into clinically usable drugs due to the complex structures and tedious preparation process.[24] Small-molecule self-reporting photosensitizers can also be developed without conjugating additional fluorescent dyes to self-report the apoptosis process induced by PDT. Recently, a self-reporting photosensitizer was developed to monitor the apoptosis process *in situ* based on the fluorescence migration of the photosensitizer from mitochondria to the

[a] Key Laboratory of Synthetic and Biological Colloids, Ministry of Education, School of Chemical and Material Engineering, Jiangnan University, Wuxi 214122, China. E-mail: xpyan@jiangnan.edu.cn
[b] Institute of Analytical Food Safety, School of Food Science and Technology, Jiangnan University, Wuxi 214122, China
[c] State Key Laboratory of Food Science and Technology, Jiangnan University, Wuxi 214122, China

† Electronic supplementary information (ESI) available. See DOI: 10.1039/d1tb02097h

nucleus.[19] However, this photosensitizer cannot provide feedback on the effect of PDT *in vivo* because the state of cells (living or dead) during PDT cannot be differentiated. To endow a small-molecule photosensitizer with the capability to self-report the PDT process *in vivo*, a self-reporting photosensitizer with tunable fluorescence intensity was also reported.[24] This photosensitizer showed weak fluorescence in living cells before PDT and lights up the nucleus of dead cells after PDT. However, this self-reporting photosensitizer only employed the change of single emission to monitor cell death, which can be disturbed by the uneven distribution of the photosensitizer and the instability of the light source.[25] To overcome the above shortcomings, it is essential to develop a dynamic dual-color mode for visual distinguishing of the state of cells. In this way, living and dead cells can be discriminated by a significant change in the emission color with a better diagnostic effect than the common single-color mode.

Herein, we report a unique self-reporting photosensitizer **TPA-3PyA+** enabling simultaneous PDT and real-time monitoring of the phototheranostic process in a dynamic dual-color mode. **TPA-3PyA+** comprises a twisted triphenylamine (TPA) unit (electron donor), three benzene ring units (π bridge) and three cyanovinyl-pyridinium (PyA) units (electron acceptor). This electron donor-π bridge-electron acceptor (D–π–A) structure endows **TPA-3PyA+** with efficient $^1O_2$ production with a high quantum yield (124%) in an aqueous solution. **TPA-3PyA+** can stain living cells with dual-color fluorescence mainly in the cytoplasm. Moreover, the emission color, intensity and intracellular location of **TPA-3PyA+** simultaneously change with the degree of cell death upon continuous light irradiation, allowing **TPA-3PyA+** to monitor the real-time PDT process *in situ*. More importantly, **TPA-3PyA+** can light up the nucleus of dead cells after PDT only with green fluorescence, suggesting that living and dead cells can be obviously distinguished by observing the emission color of **TPA-3PyA+**. This unique optical property of **TPA-3PyA+** can effectively avoid the interference of tracking cell death by observing the change in fluorescence intensity in the single-color mode. In addition, **TPA-3PyA+** exhibits effective inhibition of the growth of tumors *in vivo*. This work provides a new strategy to design ideal self-reporting photosensitizers for effective cancer theranostics.

## Results and discussion

### Design and synthesis of the self-reporting photosensitizer TPA-3PyA+

Fig. 1a shows the design of the new self-reporting photosensitizer **TPA-3PyA+** for simultaneous PDT and real-time monitoring of the phototheranostic process in a dynamic dual-color mode. **TPA-3PyA+** was constructed from a twisted triphenylamine unit (D), three benzene ring units (π) and three cyanovinyl-pyridinium units (A) to possess a twisted D–π–A structure. A twisted D–π–A system was included as it enables flexible emission behavior in different media such as different emission color and intensity due to the twisted intramolecular charge transfer (TICT) effect,[26] while the cationic pyridinium group is included to give the capacity of **TPA-3PyA+** for the interaction with organelles or biomacromolecules (such as proteins or DNA) to show the enhancement of fluorescence.[27–30] Thus, the designed amphiphilic cationic **TPA-3PyA+** enables cell staining with dual color (NIR and green) emissions once interacting with organelles or proteins in cytoplasm and DNA in the nucleus, respectively, mainly due to the TICT effect. In addition, the designed D–π–A structure can be beneficial to ROS generation due to the small singlet–triplet energy gap ($\Delta E_{ST}$ = 0.21 eV) (Fig. S1, ESI†).[31] **TPA-3PyA+** with the D–π–A system and multiple pyridinium groups not only exhibit good capacity to generate ROS for killing cancer cells but also to monitor cell apoptosis process for effective cancer theranostics.[19,24] Thus, this new photosensitizer can achieve simultaneous PDT and real-time monitoring phototheranostic process in a dynamic dual-color mode.

**TPA-3PyA+** was facilely prepared *via* three-step reactions with a total yield of 75% (Fig. 1b). Briefly, Compound **1** was synthesized *via* the Suzuki–Miyaura coupling reaction using commercially available 4-(4,4,5,5-tetramethyl-1,3,2-dioxaborolan-2-yl)benzaldehyde and tris(4-bromophenyl)amine as starting materials. Compound **2** was obtained *via* the condensation reaction between compound **1** and 4-pyridylacetonitrile. Finally, compound **2** was methylated to gain the product **TPA-3PyA+**. The structures of new compounds **2** and **TPA-3PyA+** were verified by $^1$H NMR, $^{13}$C NMR and ESI-HRMS spectroscopy (Fig. S2–S7, ESI†).

### Optical properties of TPA-3PyA+

The optical properties of **TPA-3PyA+** were firstly investigated. **TPA-3PyA+** was soluble in DMSO and DMF and showed good stability at room temperature (Fig. S8, ESI†). A pure organic solvent DMSO was used as a good solvent while the aqueous solution was explored as a poor solvent in which nanoaggregates could be formed to test the optical properties of **TPA-3PyA+** in different states (Fig. S9, ESI†). **TPA-3PyA+** showed wide absorption in the visible region both in DMSO and aqueous solution with the maximum absorption at 487 nm (Fig. S10a, ESI†), but exhibited almost no fluorescence both in DMSO and aqueous solution (Fig. S10b, ESI†), revealing that **TPA-3PyA+** possessed a strong TICT effect due to the rotatable D–π–A structure.[26]

Based on the molecular design, **TPA-3PyA+** enables dual-color fluorescence emission under certain conditions. So, we then investigated the optical behavior of **TPA-3PyA+** in the presence of biomacromolecules such as bovine serum albumin (BSA) and calf thymus DNA (ctDNA). We found that the fluorescence **TPA-3PyA+** turned on after interactions with BSA or ctDNA (Fig. 2a and b). BSA and ctDNA enabled **TPA-3PyA+** to emit NIR fluorescence (734 nm) and green fluorescence (547 nm), respectively, indicating that **TPA-3PyA+** possessed the potential to stain cells in a dual-color mode.

The emissive behaviors of molecules with the TICT effect can be influenced by the surrounding environment and molecular conformation.[26] Firstly, BSA and other various proteins are usually negatively charged and amphipathic. Cationic **TPA-3PyA+**

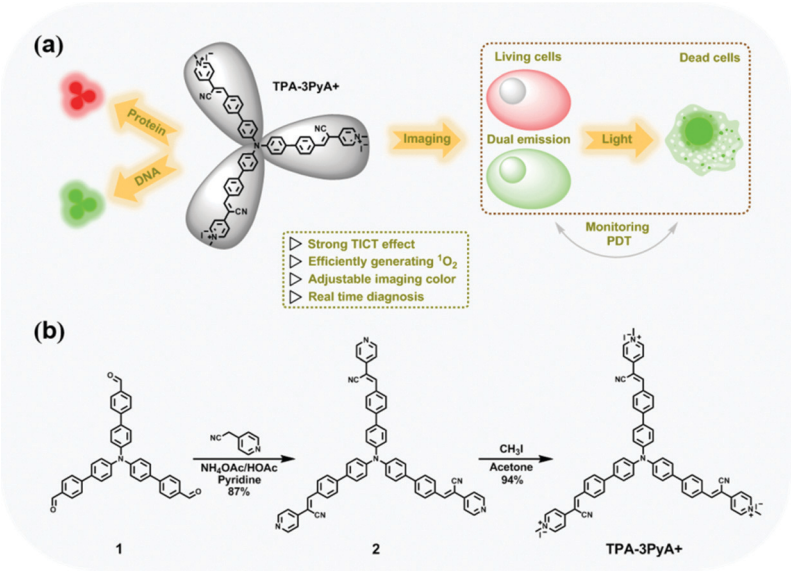


Fig. 1 (a) Illustration for the molecular structure and characteristics of the developed self-reporting photosensitizer **TPA-3PyA+**. (b) Synthetic route for **TPA-3PyA+**.

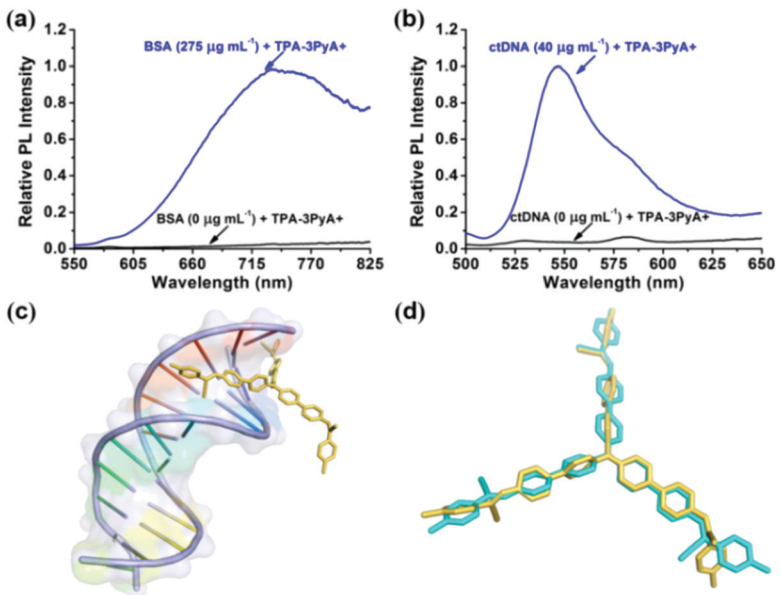


Fig. 2 Photoluminescence (PL) spectra of **TPA-3PyA+** (20 μM) in DMSO/water (1/99, v/v) with different concentrations of BSA (a) and ctDNA (b). (c) Molecular modeling for the interaction of **TPA-3PyA+** with a B-DNA dodecamer (PDB ID: 1BNA). (d) Molecular modeling of **TPA-3PyA+**: superposition of the docking pose in DNA (yellow-orange) and the stable conformation without DNA (cyan).

could effectively combine with BSA through electrostatic and hydrophobic interactions to form nanoparticles (Fig. S11a, ESI†). The formation of nanoparticles reduced the interaction between **TPA-3PyA+** and water in the system, thereby the surrounding environmental polarity of **TPA-3PyA+** in aqueous solution decreased and the TICT effect of **TPA-3PyA+** was reduced, leading to the NIR fluorescence generation of **TPA-3PyA+**. In addition, similar NIR fluorescence "turn-on" phenomenon was also observed for **TPA-3PyA+** in the aqueous solution in the presence of another negatively charged amphiphilic macromolecule 1,2-distearoyl-*sn*-glycero-3-phosphoethanolamine-*N*-[methoxy(polyethylene glycol)-2000] (DSPE-PEG$_{2000}$) (Fig. S12, ESI†). Secondly, molecules with pyridine salt groups could bind with DNA through electrostatic interactions and groove binding.[32] **TPA-3PyA+** could also interact with ctDNA to form nanoparticles (Fig. S11b, ESI†). Molecular docking studies were therefore carried out to explore the interactions between **TPA-3PyA+** and DNA (Fig. 2c and d). **TPA-3PyA+** could insert into the groove of DNA with a twist

 

conformation and the polarity of the surrounding environment of **TPA-3PyA+** further decreased. Therefore, ctDNA made **TPA-3PyA+** emit a shorter emission than BSA.

### Photosensitive properties of TPA-3PyA+

The effective dual-color emission characteristics of **TPA-3PyA+** prompted us to investigate its photosensitive performances. For this purpose, 9,10-anthracenediyl-bis(methylene) dimalonic acid (ABDA) was selected as the $^1O_2$ indicator, whose absorbance decreased after oxidation by $^1O_2$. We used DMSO/water mixture (1/99, v/v) as a solvent in which nanoaggregates could be formed to evaluate the performance of **TPA-3PyA+** for the generation of $^1O_2$. DMSO (good solvent) was not considered as a solvent because **TPA-3PyA+** existed as a discrete molecular state and gave no generation of $^1O_2$ (Fig. S13, ESI†).

**TPA-3PyA+** made the absorbance of ABDA in DMSO/water mixture (1/99, v/v) decrease quickly upon irradiation for 80 seconds (Fig. 3a), while only light irradiation led to no change in the absorbance of ABDA (Fig. 3b), indicating the effective $^1O_2$ generation of **TPA-3PyA+** in the aggregate state. The $^1O_2$ quantum yield of **TPA-3PyA+** was determined to be 124% with a commercial photosensitizer Rose Bengal (RB) as the reference ($\Phi_{RB}$ = 75% in water) (Fig. 3c, d and Fig. S14, ESI†). These results reveal that the energy decay of the molecular excited state *via* non-radiative pathways could be effectively restrained in the aggregate state.[31] Therefore, **TPA-3PyA+** possessed the aggregation-enhanced photosensitive performance. Compared to most traditional photosensitizers with poor $^1O_2$ generation in the physiological environment due to the formation of aggregates,[33] **TPA-3PyA+** had the better potential for PDT.

Encouraged by the above attractive optical and photosensitive properties of **TPA-3PyA+**, we then evaluated the dark-toxicity and phototoxicity of **TPA-3PyA+** *in vitro* by a classic 3-(4,5-dimethylthiazol-2-yl)-2,5-diphenyltetrazolium bromide (MTT) method. HeLa cells were selected as a model and incubated with different concentrations of **TPA-3PyA+** for 24 h without white light irradiation to investigate the dark toxicity of **TPA-3PyA+**. The cell viability was still over 90% even in the presence of 40 μM **TPA-3PyA+**, revealing that **TPA-3PyA+** possessed good biocompatibility (Fig. 3e). We then tested the phototoxicity of **TPA-3PyA+** under different light doses (Fig. 3f). Dramatically, there was about 50% of cells killed in the presence of 30 μM **TPA-3PyA+** under a small light dose (50 mW cm$^{-2}$, 30 min), and over 80% of cells destroyed under a light dose (90 mW cm$^{-2}$, 30 min). In addition, **TPA-3PyA+** also showed negligible dark-toxicity but obvious phototoxicity towards SCC-7 cells (Fig. S15, ESI†). Meanwhile, we also detected the ROS production abilities of **TPA-3PyA+** in living cells using DCFH-DA as an indicator, whose green fluorescence could be turned on upon reacting with ROS. As a result, the cells showed strong green fluorescence (Fig. S16, ESI†). These results further confirmed that **TPA-3PyA+** is an effective photosensitizer for PDT. Furthermore, we applied a commercial photosensitizer (Ce6) to further show the PDT performance of **TPA-3PyA+**. Ce6 showed a better anti-proliferation ability than **TPA-3PyA+** (Fig. S17, ESI†). We found that **TPA-3PyA+** showed different fluorescence quantum yields and $^1O_2$ quantum yields under various conditions (Fig. S18, S19 and Table S1, ESI†). This may affect the PDT performance of **TPA-3PyA+** in living cells that possess a complex microenvironment.

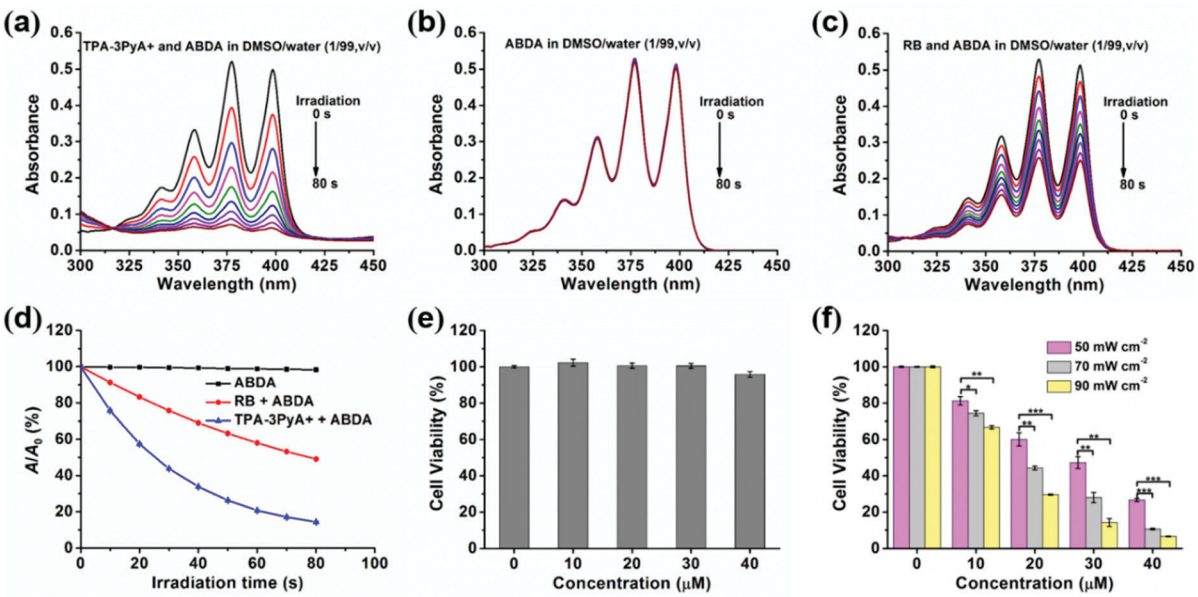


Fig. 3 UV-vis spectra of ABDA under white light irradiation (50 mW cm$^{-2}$) in DMSO/water mixture (1/99, v/v): (a) ABDA + **TPA-3PyA+**; (b) only ABDA; (c) ABDA + RB. (d) Degradation rates of ABDA in the presence of different PSs under white light irradiation, where $A_0$ and $A$ are the absorbances of ABDA at 378 nm before and after irradiation, respectively. [ABDA] = 50 μM; [**TPA-3PyA+**] = [RB] = 2 μM. Time interval for acquiring the UV-vis spectra: 10 s. (e) Cell viability of HeLa cells treated with different concentrations of **TPA-3PyA+** in dark. (f) Cell viability of HeLa cells treated with different concentrations of **TPA-3PyA+** under various doses of light irradiation (The experiments were repeated three times. *, **, and *** represent $p < 0.05$, $p < 0.01$, and $p < 0.001$, respectively).

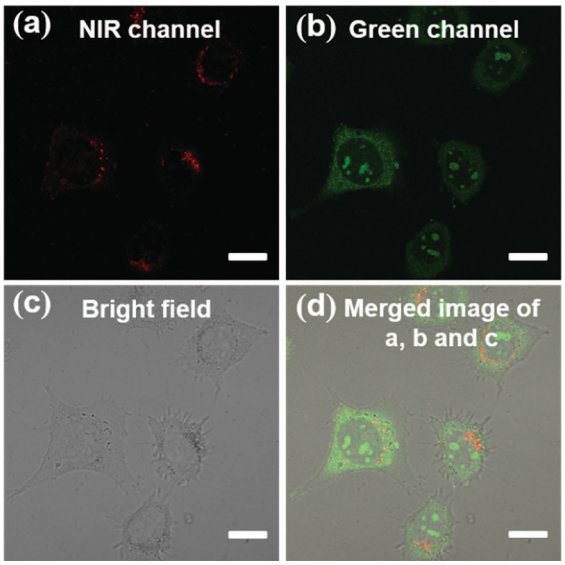


Fig. 4 Confocal images of HeLa cells stained with 40 μM **TPA-3PyA+**, scale bar: 15 μm ($\lambda_{ex}$ = 488 nm, NIR channel: >600 nm; green channel: 500–600 nm).

### Cell imaging and imaging-guided PDT performance of TPA-3PyA+

We next investigated cell imaging and imaging-guided PDT performance of **TPA-3PyA+** *in vitro*. Notably, **TPA-3PyA+** could effectively stain HeLa cells with dual-color emission (Fig. 4 and Fig. S20, ESI†). The green fluorescence almost lighted up whole cells, and the NIR fluorescence mainly appeared in the cytoplasm. Colocalization experiments for HeLa cells co-incubated with **TPA-3PyA+** and organelle trackers showed that **TPA-3PyA+** could not specially stain organelles such as mitochondria and lysosomes in HeLa cells (Fig. S21, ESI†).

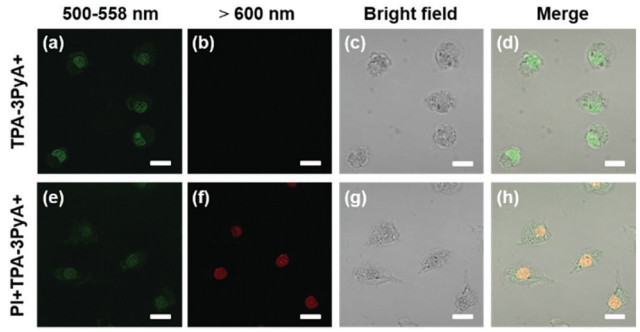


Fig. 6 Confocal images of HeLa cells after white light irradiation (70 mW $cm^{-2}$, 30 min): (a–d) the cells incubated with **TPA-3PyA+** (40 μM); (e–h) the cells co-incubated with **TPA-3PyA+** (40 μM) and PI (100 μg $mL^{-1}$). $\lambda_{ex}$ = 488 nm. Scale bar: 15 μm.

Further investigation on the self-reporting capacity of **TPA-3PyA+** for PDT-induced apoptosis monitoring revealed that the green fluorescence gradually transferred from the cytoplasm to the nucleus during laser irradiation ($\lambda_{ex}$ = 488 nm, 4% laser power) accompanied by an increase in emission intensity (Fig. 5f–j and Fig. S22, S23, ESI†) likely because **TPA-3PyA+** could effectively bond with DNA in the nucleus and exhibited the fluorescence-enhanced phenomenon during apoptosis. Meanwhile, the morphology and structure integrity of the cells significantly changed (Fig. 5k–o). In addition, the emission intensity of the NIR fluorescence gradually decreased during PDT mainly because the interaction between **TPA-3PyA+** and proteins was reduced. Consequently, **TPA-3PyA+** not only possessed effective PDT performance for cell apoptosis under continuous laser irradiation but also had the self-reporting capacity for real-time apoptosis monitoring in a dynamic dual-color mode.

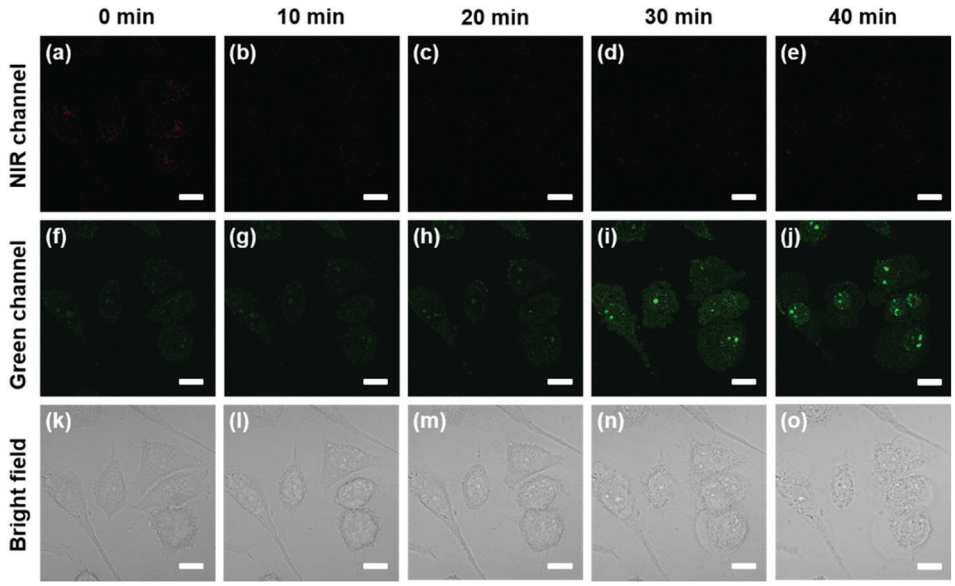


Fig. 5 Real-time confocal imaging of HeLa Cells under continuous laser irradiation ($\lambda_{ex}$ = 488 nm, 4% laser power) stained with 40 μM **TPA-3PyA+**. NIR channel: >600 nm; Green channel: 500–600 nm. Scale bar: 15 μm.

 

To further investigate the PDT performance of **TPA-3PyA+**, HeLa cells were co-incubated with **TPA-3PyA+** and propidium iodide (PI), a nuclear dye only for staining dead cells with red fluorescence (Fig. S24, ESI†). Laser irradiation gave no red fluorescence in the cells incubated only with PI, indicating that only laser irradiation did not cause apoptosis. In contrast, the nucleus of the cells co-incubated with **TPA-3PyA+** and PI showed strong red fluorescence after continuous irradiation for 30 min, further showing that **TPA-3PyA+** possessed effective photosensitive performance for killing cells under laser irradiation.

We also investigated the PDT effect of **TPA-3PyA+** under white light irradiation due to its wide absorption in the visible region. The results in Fig. 6 and Fig. S25 (ESI†) show that **TPA-3PyA+** is mainly located in the nucleus of the cells and only stained the cells with obvious green fluorescence. In addition, the almost loss of cell structure integrity was seen from the bright field images. These cells were further incubated with PI to confirm the cell viability and the intracellular location of **TPA-3PyA+**. PI obviously stained the nucleus of cells with red fluorescence, indicating the death of cells due to the PDT effect of **TPA-3PyA+**. Meanwhile, **TPA-3PyA+** and PI co-located in the nucleus. Furthermore, cell imaging of fixed HeLa cells with **TPA-3PyA+** showed that only green fluorescence was mainly located in the nucleus (Fig. S26, ESI†). The above results revealed that **TPA-3PyA+** mainly stained the nucleus of the dead cells, and also had good PDT performance under white light irradiation.

### *In vivo* antitumor performance of TPA-3PyA+

We further evaluated the *in vivo* antitumor performance of **TPA-3PyA+** under white light irradiation (Fig. 7a, c, d and Fig. S27, ESI†). BALB/c mice of subcutaneous SCC-7 tumor models were established for *in vivo* study. The mice were randomly divided into four groups. Two groups (“**TPA-3PyA+**” and “**TPA-3PyA+** + light”) were injected intratumorally with a 5% glucose solution (GS) of **TPA-3PyA+** (100 μL, 1 mg $mL^{-1}$). Another two groups (“GS” and “GS + light”) were injected with 100 uL 5% GS. The “GS” and “GS + light” groups showed fast tumor growth, suggesting that only GS or light made no influence on tumor growth. The “**TPA-3PyA+**” group also exhibited obvious tumor growth without light irradiation, indicating that **TPA-3PyA+** possessed good biocompatibility. However, the tumor growth of the “**TPA-3PyA+** + light” group was significantly inhibited

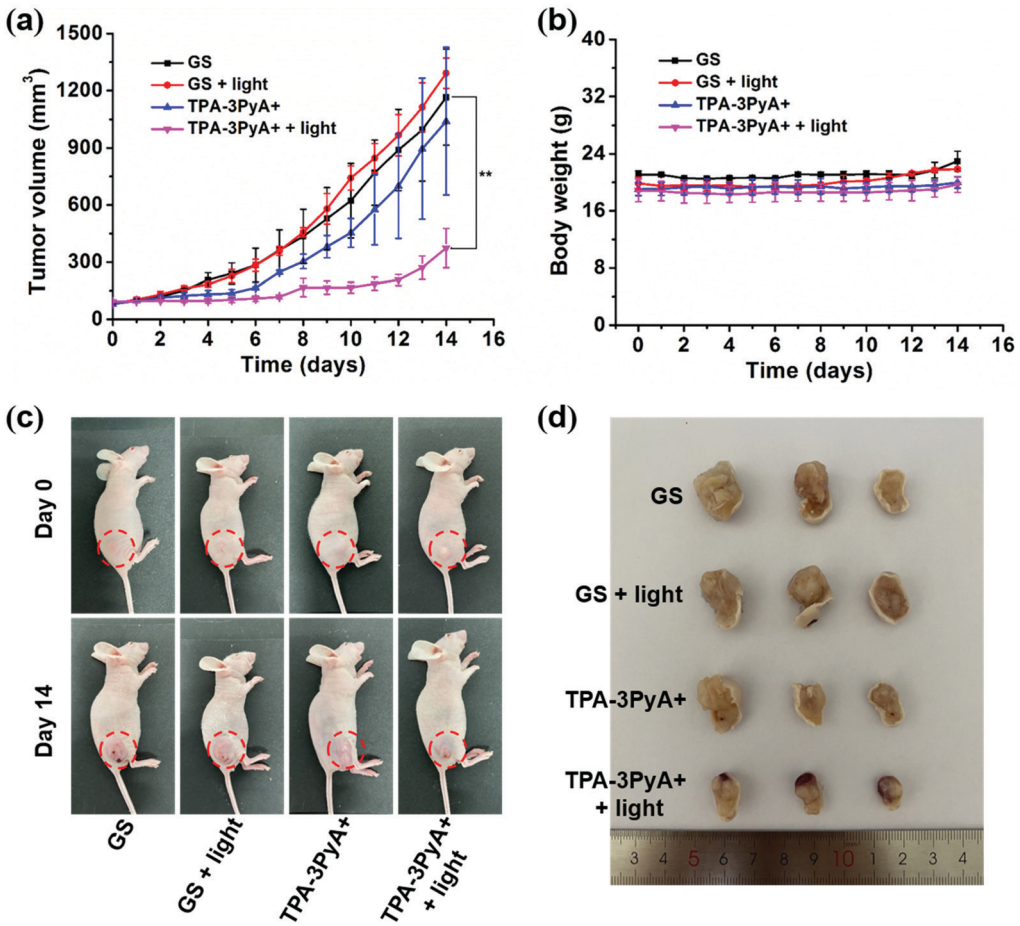


Fig. 7 (a) Tumor growth curves of mice with different treatments ($n$ = 3 for each group, **, $p < 0.01$). (b) Body weight of mice with different treatments during 14 days. (c) Representative photos of mice with different treatments at the beginning (day 0) and end (day 14) of treatments. (d) Photos of the tumors of mice at day 14 after different treatments.

after light irradiation. In addition, H&E staining of the tumor slice showed obvious void spaces and karyopyknosis in the "**TPA-3PyA+** + light" group compared with other groups, revealing that **TPA-3PyA+** had the good PDT efficacy (Fig. S28, ESI†). Furthermore, a small change in mice body weight during PDT and H&E staining of major organ slices of mice further revealed the good biocompatibility of **TPA-3PyA+** (Fig. 7b and Fig. S28, ESI†).

## Conclusions

We have reported a unique self-reporting photosensitizer **TPA-3PyA+** with good PDT performance as well as the capacity for monitoring the PDT process in a dynamic dual-color mode. Its TICT effect enables the designed amphiphilic cationic **TPA-3PyA+** to stain living cells with dual-color (NIR and green) fluorescence. **TPA-3PyA+** can migrate from the cytoplasm into the nucleus accompanied by the enhancement of the green fluorescence and the decrease in the NIR fluorescence as the cells gradually die upon continuous light irradiation. This unique feature allows **TPA-3PyA+** real-time monitor PDT process *in situ*. Moreover, the capability of **TPA-3PyA+** to light up only the nucleus of dead cells with green fluorescence permits its application for distinguishing living and dead cells. In addition, the designed D–π–A structure gives **TPA-3PyA+** excellent PDT performance. Thus, the prepared **TPA-3PyA+** is promising for simultaneous PDT and real-time monitoring phototheranostic process in a dynamic dual-color mode. We believe that this type of self-reporting system with a dynamic dual-color mode will encourage us to develop more ideal phototheranostic modalities and the study is underway.

## Experimental section

### Synthesis of compound 2

A mixture of compound 1 (0.20 g, 0.36 mmol), 2-(pyridin-4-yl)acetonitrile (0.19 g, 1.62 mmol), and ammonium acetate (0.028 g, 0.36 mmol) in a solution of 2 mL glacial acetic acid and 10 mL pyridine was stirred at room temperature for 24 h. Then, water was added to the above solution to get orange red solid. The solid was filtered off, washed with water for several times, and purified by column chromatography with DCM/$CH_3OH$ (45/1, v/v) as the eluent to obtain compound **2** as an orange red powder (0.27 g, 87%). $^1$H NMR (400 MHz, $CDCl_3$, ppm): $\delta$ 8.72 (dd, $J$ = 1.6 Hz, $J$ = 4.8 Hz, 6H, Ar*H*), 8.05 (d, $J$ = 8.4 Hz, 6H, Ar*H*), 7.76 (s, 3H, C*H*), 7.75 (d, $J$ = 8.0 Hz, 6H, Ar*H*), 7.63 (d, $J$ = 8.4 Hz, 6H, Ar*H*), 7.60 (dd, $J$ = 1.6 Hz, $J$ = 4.4 Hz, 6H, Ar*H*), 7.30 (d, $J$ = 8.8 Hz, 6H, Ar*H*). $^{13}$C NMR (100 MHz, $CDCl_3$, ppm): $\delta$ 150.6, 147.4, 144.6, 143.6, 142.0, 134.4, 131.5, 130.6, 128.2, 127.2, 124.7, 119.9, 117.2, 108.5. HRMS (ESI): $m/z$ for $C_{60}H_{40}N_7^+$ ($[M + H]^+$): calc. 858.3340; found 858.3401.

### Synthesis of TPA-3PyA+

A solution of compound **2** (0.050 g, 0.058 mmol) and iodomethane (0.2 mL) in acetone (20 mL) was allowed to stir under nitrogen at 60 °C for 12 h. After removing acetone in vacuum, the residue was washed sequentially with ethyl acetate and methanol, and dried under reduced pressure to obtain the product **TPA-3PyA+** as a purple-black solid (0.070 g, 94%). $^1$H NMR (400 MHz, DMSO-$d_6$, ppm): $\delta$ 9.06 (d, $J$ = 6.8 Hz, 6H, Ar*H*), 8.77 (s, 3H, C*H*), 8.44 (d, $J$ = 6.8 Hz, 6H, Ar*H*), 8.23 (d, $J$ = 8.4 Hz, 6H, Ar*H*), 8.03 (d, $J$ = 8.4 Hz, 6H, Ar*H*), 7.89 (d, $J$ = 8.8 Hz, 6H, Ar*H*), 7.28 (d, $J$ = 8.4 Hz, 6H, Ar*H*), 4.35 (s, 9H, $CH_3$). $^{13}$C NMR (100 MHz, DMSO-$d_6$, ppm): $\delta$ 151.0, 149.0, 147.0, 145.8, 143.7, 133.3, 131.5, 131.1, 128.4, 126.9, 124.5, 123.1, 116.5, 104.5, 47.4. HRMS (ESI): $m/z$ for $C_{63}H_{48}N_7^{3+}$ ($[M]^{3+}$): calc. 300.7985; found 300.7984.

## Ethical statement

All animal experiments were carried out under the permission and guidance of the Animal Ethics Committee of Jiangnan University.

## Conflicts of interest

There are no conflicts of interest to declare.

## Acknowledgements

The authors are thankful for the financial support from National Natural Science Foundation of China (No. 21934002, 21804057, and 21804056), Postgraduate Research & Practice Innovation Program of Jiangsu Province (No. KYCX20_1775), and Natural Science Foundation of Jiangsu Province, China (No. BK20180584 and BK20180581), National First-class Discipline Program of Food Science and Technology (No. JUFSTR20180301), and Collaborative Innovation Center of Food Safety and Quality Control in Jiangsu Province.

## References

1 H. Sung, J. Ferlay, R. L. Siegel, M. Laversanne, I. Soerjomataram, A. Jemal and F. Bray, *Ca-Cancer J. Clin.*, 2021, **71**, 209–249.
2 S. S. Kelkar and T. M. Reineke, *Bioconjugate Chem.*, 2011, **22**, 1879–1903.
3 S. Mura and P. Couvreur, *Adv. Drug Delivery Rev.*, 2012, **64**, 1394–1416.
4 M. Gao, F. Yu, C. Lv, J. Choo and L. Chen, *Chem. Soc. Rev.*, 2017, **46**, 2237–2271.
5 Kenry, K. C. Chong and B. Liu, *Acc. Chem. Res.*, 2019, **52**, 3051–3063.
6 J. Zhou, L. Rao, G. Yu, T. R. Cook, X. Chen and F. Huang, *Chem. Soc. Rev.*, 2021, **50**, 2839–2891.
7 J. Bhaumik, A. K. Mittal, A. Banerjee, Y. Chisti and U. C. Banerjee, *Nano Res.*, 2015, **8**, 1373–1394.
8 Y. Cai, W. Si, W. Huang, P. Chen, J. Shao and X. Dong, *Small*, 2018, **14**, 1704247.

 

9 C. Chen, H. Ou, R. Liu and D. Ding, *Adv. Mater.*, 2020, **32**, 1806331.
10 W. Hu, P. N. Prasad and W. Huang, *Acc. Chem. Res.*, 2021, **54**, 697–706.
11 J. P. Celli, B. Q. Spring, I. Rizvi, C. L. Evans, K. S. Samkoe, S. Verma, B. W. Pogue and T. Hasan, *Chem. Rev.*, 2010, **110**, 2795–2838.
12 J. X. Zhang, H. Li, C. F. Chan, R. Lan, W. L. Chan, G. L. Law, W. K. Wong and K. L. Wong, *Chem. Commun.*, 2012, **48**, 9646–9648.
13 J. Lin, S. Wang, P. Huang, Z. Wang, S. Chen, G. Niu, W. Li, J. He, D. Cui, G. Lu, X. Chen and Z. Nie, *ACS Nano*, 2013, **7**, 5320–5329.
14 Y. Yuan, C. J. Zhang, M. Gao, R. Zhang, B. Z. Tang and B. Liu, *Angew. Chem., Int. Ed.*, 2015, **54**, 1780–1786.
15 Z. Zhang, W. Xu, M. Kang, H. Wen, H. Guo, P. Zhang, L. Xi, K. Li, L. Wang, D. Wang and B. Z. Tang, *Adv. Mater.*, 2020, **32**, 2003210.
16 Q. Wang, J. Xu, R. Geng, J. Cai, J. Li, C. Xie, W. Tang, Q. Shen, W. Huang and Q. Fan, *Biomaterials*, 2020, **231**, 119671.
17 P. Cheng and K. Pu, *ACS Appl. Mater. Interfaces*, 2020, **12**, 5286–5299.
18 R. Chennoufi, H. Bougherara, N. Gagey-Eilstein, B. Dumat, E. Henry, F. Subra, F. Mahuteau-Betzer, P. Tauc, M. P. Teulade-Fichou and E. Deprez, *Chem. Commun.*, 2015, **51**, 14881–14884.
19 T. Zhang, Y. Li, Z. Zheng, R. Ye, Y. Zhang, R. T. K. Kwok, J. W. Y. Lam and B. Z. Tang, *J. Am. Chem. Soc.*, 2019, **141**, 5612–5616.
20 P. Wang, F. Zhou, K. Guan, Y. Wang, X. Fu, Y. Yang, X. Yin, G. Song, X. B. Zhang and W. Tan, *Chem. Sci.*, 2019, **11**, 1299–1306.
21 Z. Zhang, R. Wang, R. Luo, J. Zhu, X. Huang, W. Liu, F. Liu, F. Feng and W. Qu, *ACS Nano*, 2021, **15**, 5366–5383.
22 Y. Yuan, C. J. Zhang, S. Xu and B. Liu, *Chem. Sci.*, 2016, **7**, 1862–1866.
23 T. Xiong, M. Li, Y. Chen, J. Du, J. Fan and X. Peng, *Chem. Sci.*, 2020, **12**, 2515–2520.
24 Y. Gao, X. Wang, X. He, Z. He, X. Yang, S. Tian, F. Meng, D. Ding, L. Luo and B. Z. Tang, *Adv. Funct. Mater.*, 2019, **29**, 1902673.
25 L. Yuan, W. Lin, K. Zheng and S. Zhu, *Acc. Chem. Res.*, 2013, **46**, 1462–1473.
26 S. Sasaki, G. P. C. Drummen and G.-I. Konishi, *J. Mater. Chem. C*, 2016, **4**, 2731–2743.
27 G. R. Rosania, J. W. Lee, L. Ding, H.-S. Yoon and Y.-T. Chang, *J. Am. Chem. Soc.*, 2003, **125**, 1130–1131.
28 Y. Liu, J. Niu, W. Wang and W. Lin, *Anal. Chem.*, 2019, **91**, 1715–1718.
29 Y. Huang, X. You, L. Wang, G. Zhang, S. Gui, Y. Jin, R. Zhao and D. Zhang, *Angew. Chem., Int. Ed.*, 2020, **59**, 10042–10051.
30 Q. Jiang, X. Xu, P. A. Yin, K. Ma, Y. Zhen, P. Duan, Q. Peng, W. Q. Chen and B. Ding, *J. Am. Chem. Soc.*, 2019, **141**, 9490–9494.
31 F. Hu, S. Xu and B. Liu, *Adv. Mater.*, 2018, **30**, 1801350.
32 Y. Gao, Z. He, X. He, H. Zhang, J. Weng, X. Yang, F. Meng, L. Luo and B. Z. Tang, *J. Am. Chem. Soc.*, 2019, **141**, 20097–20106.
33 J. F. Lovell, T. W. B. Liu, J. Chen and G. Zheng, *Chem. Rev.*, 2010, **110**, 2839–2857.